Two-step, oxygen-free conversion of methane over supported NiB amorphous alloy catalysts

Yong Lu [a], Jitao Li [a] and Jianyi Lin [b,*]

[a] *Chemical and Process Engineering Center, National University of Singapore, Singapore, 117576*
[b] *Department of Physics, National University of Singapore, Singapore, 119260*
E-mail: phylinjy@nus.edu.sg

Received 1 May 2001; accepted 27 July 2001

NiB amorphous alloy and Ni catalysts supported on HMCM-22, HZSM-5, HY, γ-Al_2O_3 and SiO_2 were prepared, respectively, by the chemical reduction method and the standard incipient wetness impregnation method. These catalysts were examined for catalytic performance in the two-step conversion of CH_4 to produce hydrogen and higher hydrocarbons. All catalysts give similar methane conversion and yields of hydrogen and H-deficient carbon-containing species in *step I*. In the subsequent hydrogenation step (*step II*), they have similar carbon conversion, however, the yield of C_2 and C_3 hydrocarbons depends greatly on the nature of the metal particles and support acidity. Supported NiB amorphous alloy catalysts offer higher yield of C_2 and C_3 hydrocarbons than the corresponding Ni catalysts, due to their unique properties: nanoscale size, long-range disorder in structure, and electron-deficiency. Of the zeolite supported catalysts, HMCM-22 and HZSM-5 supported catalysts produce higher yield of C_2 and C_3 hydrocarbons than the zeolite HY supported catalyst because of stronger acidity of the supports. A NiB/HMCM-22 catalyst shows a rather slow deactivation during a multiple reaction cycles test. High temperature favors CH_4 decomposition and H_2 production in *step I*, but makes the subsequent hydrogenation of carbon formed from CH_4 decomposition difficult. The nature of the carbons formed from CH_4 decomposition was also studied by XPS and TEM combined with H_2-TPSR.

KEY WORDS: two-step conversion of methane; NiB amorphous alloy catalyst; hydrogenation; higher hydrocarbon formation; coke

1. Introduction

Methane activation and its conversion into more useful chemicals are among the most exciting catalysis problems of the last decade. By far the most promising and explored routes, such as oxidative coupling to ethylene, direct oxidation to methanol, *etc*. cannot give good selectivity at acceptable yields of conversion [1].

Hydrogenation of carbon species formed from decomposition of methane to higher hydrocarbons is one of the recent achievements in the research of methane application [2,3]. The idea is to separate the CH_4 conversion reaction into two steps by time and temperature, with the first being the catalytic decomposition of methane on metal, followed by the subsequent hydrogenation of the carbon species at the same or lower temperatures:

$$CH_4 \rightarrow C_{ads}/[CH_x]_{ads} + (2 - x/2)H_2 \qquad \text{(step I)}$$

$$C_{ads}/[CH_x]_{ads} + H_2 \rightarrow C_nH_{2n+2},\ C_nH_{2n},\ \text{aromatics, } \textit{etc.} \qquad \text{(step II)}$$

Clearly, this process shows advantages in production of higher hydrocarbons from CH_4 decomposition with 100% atom utilization. Belgued *et al.* [2] reported that on a standard Pt catalyst 19.3% of carbon hydrogenated with 7.9% of C_{2+} yield could be achieved in *step II* at 250 °C. Goodman [4] reported that on a Ru–Cu/SiO_2 (Cu/Ru = 0.1) catalyst ∼80% of carbon hydrogenated with ∼15% ethane selectivity could be achieved. The studies concerned with such two-step process have been extended to various group VIII metals and have been confirmed by several authors [1,5–8]. Recently, more and more attention has been attracted by the ultrafine amorphous alloy material because of its specific properties in catalysis, derived from the combination of their short-range order and long-range disorder in structure and nanoscale size [9]. In this work, supported NiB amorphous alloy catalysts prepared by the chemical reduction method were examined for catalytic performance in this stepwise CH_4 conversion and compared with supported Ni catalyst prepared by the standard incipient wetness impregnation method. Reaction results were correlated with the properties of metal particles of the catalysts and support acidity (acid type and strength) as well as specific surface area. The nature of the carbons formed from CH_4 decomposition was also studied by XPS and TEM combined with hydrogen temperature-programmed surface reactions (H_2-TPSR).

2. Experimental

2.1. Catalyst preparation and treatment

A series of supported NiB amorphous alloy catalysts with metal loading of 10 wt% were prepared by chemical reduction, using HMCM-22 zeolite (molar SiO_2/Al_2O_3 ratio 50, SA 380 m^2), HZSM-5 zeolite (molar SiO_2/Al_2O_3 ratio 60,

* To whom correspondence should be addressed.

1011-372X/01/1000-0167$19.50/0

SA 400 m^2/g), HY (SA 720 m^2/g), γ-Al_2O_3 (SA 160 m^2/g), SiO_2 (SA 400 m^2/g) as supports, respectively. Preparation procedures were as follows: 2.0 g of support was impregnated overnight with equivalent volume of an aqueous nickel chlorate solution containing 0.2 g of nickel. After drying at 100 °C and calcination at 350 °C for 2.0 h, the nickel precursor on the support was reduced by dropping an aqueous solution of KBH_4 (0.5 M) at room temperature under vigorous stirring until no bubbles were effluent. Excess KBH_4 (molar ratio of KBH_4 to Ni^{2+} is 4) was used to ensure the complete reduction of Ni^{2+} ions. As-synthesized catalyst samples were then washed thoroughly with distilled water and anhydrous ethanol in series. Finally, the catalysts were stored in anhydrous ethanol. Before the reaction, the supported amorphous alloy was purged by highly purified Ar (or N_2) flow (20 ml/min) for removing the alcohol. The desired amount of such dried sample was packed into the reactor and heated to 250 °C, maintaining this temperature for 1 h in a H_2/Ar gas mixture flow with a rate of 30 ml/min for complete removal of adsorbed alcohol. Then, the catalyst bed was heated or cooled to the appointed temperature in highly purified Ar flow.

For comparison, several supported Ni catalysts with the same metal loading of 10 wt% were also prepared by standard incipient wetness impregnation. For each preparation, 1.0 g of support was impregnated overnight with equivalent volume of an aqueous nickel chlorate solution containing 0.1 g metal. The samples were dried at 100 °C, calcined at 250 °C for 2 h, and then heated at 600 °C for another 5 h. Before the reaction, the catalyst was reduced with H_2 (15 ml/min) in flowing Ar at a total rate of 30 ml/min at 600 °C for 5 h and was heated or cooled to the appointed temperature.

2.2. Microreactor evaluation

A microreactor system consisting of a quartz tube reactor, a furnace controlled by a programmable temperature controller was used in this work. The reactor was 20 cm long with 6 mm od. The two-step conversion of methane was carried out in the temperature range between 250 and 650 °C, using 100 mg of catalyst. In *step I*, 2462 μmol of highly pure methane was allowed to flow over a catalyst bed at a flow rate of 6 ml/min for 10 min. In *step II*, the above CH_4-reacted catalyst bed was flushed thoroughly with Ar and then was hydrogenated in a hydrogen flow (6 ml/min) for 10 min. The outlet gases in *step I* and *step II* were collected, respectively, using a wet meter which can display the volume of the gases accurately and then analyzed by a GC equipped with a TCD and a FID in series. The TCD connected with a Porapak Q column (2.0 m, 60 °C) was used for the hydrogen analysis. The FID fixed with the same column was used for the hydrocarbon analysis. The amount of methane unreacted in *step I* as well as the total amount of hydrocarbons including methane formed during hydrogenation were determined from the concentration results (from GC) and gas volume. Thus, methane conversion in *step I* as well as carbon conversion and C_2 and C_3 hydrocarbons yields in *step II* could be determined on a C atom basis. H_2 yield was defined as 0.5 × moles of hydrogen/total moles of methane (introduced to the catalyst). Only traces of C_{4+} hydrocarbons could be detected during hydrogenation and hence are not mentioned further in this study.

Table 1
Ni dispersion of the individual catalysts.

Catalyst (Ni loading 10 wt%)	Dispersion (%)
NiB/HMCM-22	5.2
NiB/HZSM-5	5.4
NiB/HY	6.3
NiB/SiO_2	5.6
Ni/HMCM-22[a]	2.6
Ni/HY[a]	3.4
Ni/SiO_2[a]	3.0

[a] Pre-reduced with H_2 (15 ml/min) in flowing Ar at a total rate of 30 ml/min at 600 °C for 5 h.

2.3. Catalyst characterization

Dispersion of Ni was measured by CO dynamic pulse adsorption experiments carried out at room temperature, assuming a CO/Ni ratio of 1.0. Analysis of CO was carried out on-line with a MS (Hiden HPR 20 QMS sampling system). CO pulses (0.1 ml for each pulse) were injected until the CO peak area for such consecutive pulses was constant. The Ni dispersion of the individual catalysts is displayed in table 1.

TEM measurements of the catalysts and filamental carbons were carried out using a JEM-1200EX/9100EDAX instrument. Samples before and after reaction were ultrasonically dispersed in alcohol and spread over perforated copper grids. Several bright field TEM images of different portions of the sample were recorded at magnifications up to 100 000. Particle size and diameter of filamental carbon were determined from these micrographs.

Powder XRD patterns were recorded on Brucker AXS D8 using a scanning of 0.02°/s and an accelerating voltage of 40 kV.

XPS analyses were carried out on VG ESCALAB MKII, using a Mg Kα X-ray source (1253.6 eV, 150 W) at a constant analyzer pass energy of 20 eV. The charging effect was corrected by referring to contaminative C 1s at 284.6 eV of binding energy.

Hydrogen temperature-programmed surface reaction (H_2-TPSR) experiment was performed on the CH_4-reacted catalyst. After exposing the catalyst to the flow of CH_4 at 300 °C for 10 min, the reactor was closed and cooled to room temperature quickly using ice. Then the catalyst bed was purged by Ar to clear of CH_4. Following this the catalyst was fed with a flow of 10 vol% H_2 in Ar and thereafter was heated at a ramp of 10 °C/min up to 450 °C. The outlet gas was analyzed by an on-line MS (Hiden HPR 20 QMS sampling system) and the profiles were recorded. The MS worked with MID mode (multi-ion detection), using a Faraday detector.

3. Results and discussion

3.1. Reaction results of the isothermal two-step conversion of methane

The reaction results over NiB amorphous alloy catalysts and Ni catalysts supported on various supports are summarized in tables 2 and 3, respectively. In *step I*, all supported catalysts behave in a very similar manner in terms of CH_4 conversion and yields of H_2 and carbon at each temperature. The main carbon-containing product formed from CH_4 decomposition (*step I*) is carbon. C_2 and C_3 hydrocarbons could also be formed with a yield of no more than 0.6% in this step. With increase of the temperature, CH_4 conversion increases slowly up to 500 °C and sharply from 500 to 650 °C while the yield of C_2 and C_3 decreases by and large. This is consistent with the trend observed by several authors [4–6,10]. Note that HY supported catalysts show lower activity at various temperatures. In *step II*, all supports produce catalysts with similar conversion of carbon, however, the yield of C_2 and C_3 hydrocarbons attenuates in the following order: HMCM-22, HZSM-5 > HY > NaY, SiO_2 > γ-Al_2O_3. With increase of the temperature, conversion of the carbon formed in *step II* as well as the yield of C_2 and C_3 hydrocarbons first increases slightly and then decreases obviously. This result suggests that the optimum temperature for both CH_4 decomposition and subsequent hydrogenation is around 300 °C. Belgued *et al.* [1] also indicated that on a standard Pt catalyst the total C_{2+} production was maximum around 250–300 °C. Koerts and van Santen [3,7] showed that low temperature (<150 °C, $\Delta G < 0$) thermodynamically favors the selectivity for C_{2+} formation. Their thermodynamic analysis for this process on Co is based on bulk Co_3C formation, however, the real catalyst surface after reaction with CH_4 is quite complex beyond we can expect. So, this thermodynamic analysis has reference value rather than the justification standard. On the other hand, higher temperature (*e.g.*, 250–300 °C) may be kinetically favorable for C_{2+} formation.

The reaction results in tables 2 and 3 also suggest that carbon intermediate species from CH_4 decomposition *rapidly* transform to "inactive" carbon and this transform is accelerated greatly with increasing methane decomposition temperature. TEM measurements show that filamental carbon

Table 2
Results of the isothermal two-step conversion of CH_4 to higher hydrocarbons on a series of supported Ni catalysts in temperature range of 250–650 °C.

Support	*Step I*[a] (% moles C)				*Step II*[a] (% moles C)		
	X_{CH_4}	Y_{H_2}	$Y_{C_2-C_3}$	Y_C	X_C	Y_{C_2}	Y_{C_3}
			250 °C				
HMCM-22	1.5	0.8	0.6	0.9	53.5	5.5	3.3
HY	1.0	0.6	0.4	0.6	52.6	4.6	3.1
SiO_2	1.4	1.0	0.4	1.0	50.8	4.5	2.1
			300 °C				
HMCM-22	2.1	1.6	0.5	1.6	58.1	6.3	3.6
HZSM-5	2.0	1.0	0.4	1.0	59.8	5.9	3.2
HY	1.5	1.0	0.5	1.0	56.9	5.2	3.5
γ-Al_2O_3	2.0	1.4	0.4	1.6	55.7	2.8	1.7
SiO_2	2.1	1.8	0.3	1.8	57.1	3.1	2.1
			350 °C				
HMCM-22	2.3	2.0	0.2	2.1	52.9	3.7	2.1
HZSM-5	2.4	1.4	1.0	1.4	56.1	3.3	1.5
			400 °C				
HMCM-22	2.5	2.4	0.1	2.4	51.5	2.3	1.6
HZSM-5	2.6	2.4	0.2	2.4	50.1	2.4	1.8
HY	2.4	2.2	0.2	2.2	51.2	2.0	1.2
γ-Al_2O_3	3.1	2.8	0.3	2.7	48.8	1.6	1.3
SiO_2	3.2	3.0	0.1	3.1	50.5	1.5	1.9
			500 °C				
HMCM-22	4.9	4.8	0.1	4.8	45.3	0.8	0.7
HZSM-5	5.2	5.0	0.2	5.0	44.7	0.4	0.5
HY	2.9	2.6	0.3	2.6	45.7	0.5	0.3
γ-Al_2O_3	4.6	4.2	0.3	4.3	42.1	0.5	0.3
SiO_2	4.6	4.6	0.1	4.5	44.5	0.4	0.5
			650 °C				
HMCM-22	12.2	12.1	< 0.1	12.2	20.4	0.5	0.2
HY	4.2	4.1	0.2	4.0	25.3	0.2	0.3
SiO_2	13.0	12.6	< 0.1	13.0	21.2	0.1	0.2

[a] X: conversion; Y: yield.

Table 3
Results of the isothermal two-step conversion of CH_4 higher hydrocarbons on a series of supported NiB amorphous alloy catalysts in temperature range of 250–650 °C.

Support	*Step I*[a] (% moles C)				*Step II*[a] (% moles C)		
	X_{CH_4}	Y_{H_2}	$Y_{C_2-C_3}$	Y_C	X_C	Y_{C_2}	Y_{C_3}
			250 °C				
HMCM-22	1.8	1.0	0.7	1.1	50.9	6.2	6.6
HZSM-5	1.4	0.8	0.5	0.9	51.2	5.7	4.2
HY	1.8	1.4	0.5	1.3	50.8	5.0	3.0
γ-Al_2O_3	1.8	1.4	0.2	1.6	51.8	2.4	2.3
NaY	2.4	1.1	1.4	1.0	52.1	4.2	2.3
			300 °C				
HMCM-22	2.0	1.6	0.4	1.5	60.1	10.9	5.2
HZSM-5	1.8	1.2	0.5	1.3	58.2	10.6	5.0
HY	1.9	1.6	0.4	1.5	58.7	5.5	3.1
γ-Al_2O_3	2.2	1.6	0.5	1.7	56.7	3.6	3.0
NaY	3.0	1.6	0.7	1.6	59.6	4.2	2.8
			350 °C				
HMCM-22	2.3	2.0	0.4	1.9	55.6	5.9	2.3
HZSM-5	2.0	1.8	0.2	1.8	54.3	5.3	2.3
HY	2.0	1.8	0.2	1.8	54.9	3.6	1.6
γ-Al_2O_3	2.5	2.2	0.3	2.2	54.0	2.3	1.7
NaY	3.5	3.2	0.2	3.3	55.5	3.1	2.0
			400 °C				
HMCM-22	2.5	2.4	0.1	2.4	52.0	4.1	1.7
HZSM-5	2.1	2.0	0.1	2.0	51.5	3.6	1.2
HY	2.5	2.4	0.1	2.4	50.3	2.7	1.3
NaY	3.9	3.6	0.2	3.7	51.6	2.0	1.4
			500 °C				
HMCM-22	3.9	3.6	0.1	3.8	45.8	1.1	0.8
HZSM-5	4.6	4.5	< 0.1	4.6	45.7	0.9	0.5
HY	3.6	3.6	< 0.1	3.6	43.9	0.3	0.5
γ-Al_2O_3	4.1	4.0	0.1	4.0	41.5	0.3	0.8
NaY	4.8	4.6	0.1	4.7	44.2	0.4	0.5
			650 °C				
HMCM-22	14.2	14.0	< 0.1	14.2	22.1	0.5	0.3
γ-Al_2O_3	14.1	14.0	< 0.1	14.1	20.5	0.1	0.3
NaY	13.3	13.2	< 0.1	13.3	23.2	0.1	0.1

[a] X: conversion; Y: yield.

with a diameter of 7 nm would be formed under methane decomposition temperature higher than 500 °C. Such carbon is chemically inert and is not easy to be gasified *rapidly* via hydrogenation at temperature lower than 600 °C. It is well known that methane decomposition on reduced transition metal can result in three different kinds of surface carbon species: C_α (carbidic carbon), C_β (amorphous carbonaceous layer), and C_γ (graphite carbon). Koerts and van Santen [3,7] pointed out that carbidic (C_α) surface carbon is most suitable for the formation of C_{2+} hydrocarbons and a high selectivity for its formation can be achieved at a low carbon surface coverage. Undoubtedly, increasing CH_4 decomposition temperature not only increases the carbon surface coverage but also favors the formation of inactive carbons, *e.g.*, C_β and C_γ, even filamental carbons. This results in the decrease in the yield of C_{2+} formation with the increase in CH_4 decomposition temperature.

3.2. Comparison of NiB amorphous alloy catalysts and Ni catalysts

Carbon hydrogenated, yield of C_2 and C_3 hydrocarbons at 300 °C over supported NiB amorphous alloy and supported nickel catalysts are displayed in figure 1. Clearly, both groups of supported NiB amorphous alloy and Ni catalysts show similar conversion of carbon during hydrogenation, however, the yield of C_2 and C_3 hydrocarbons for supported NiB amorphous alloy catalysts is higher than that for corresponding Ni catalysts. For 10 wt% NiB/HMCM-22 catalyst 60.1% of carbon formed from CH_4 decomposition (*step I*) is removed via hydrogenation with 16.1% of yield of C_2 and C_3 hydrocarbons, which is comparable to those for a Ru–Cu/SiO_2 [4] and a Ru/SiO_2 [3], and is higher than that for a standard Pt catalyst reported by Belgued *et al.* [2].

In order to understand the nature of the catalytic behavior of the supported NiB amorphous alloy catalyst, catalyst

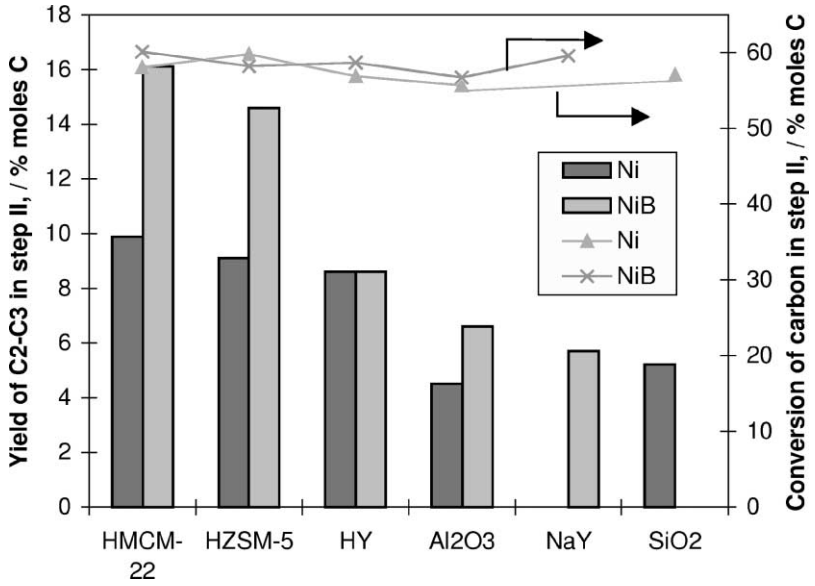

Figure 1. Carbon hydrogenated, yield of C_2 and C_3 hydrocarbons at 300 °C over supported NiB amorphous alloy and supported Ni catalysts. Data are deduced from tables 2 and 3.

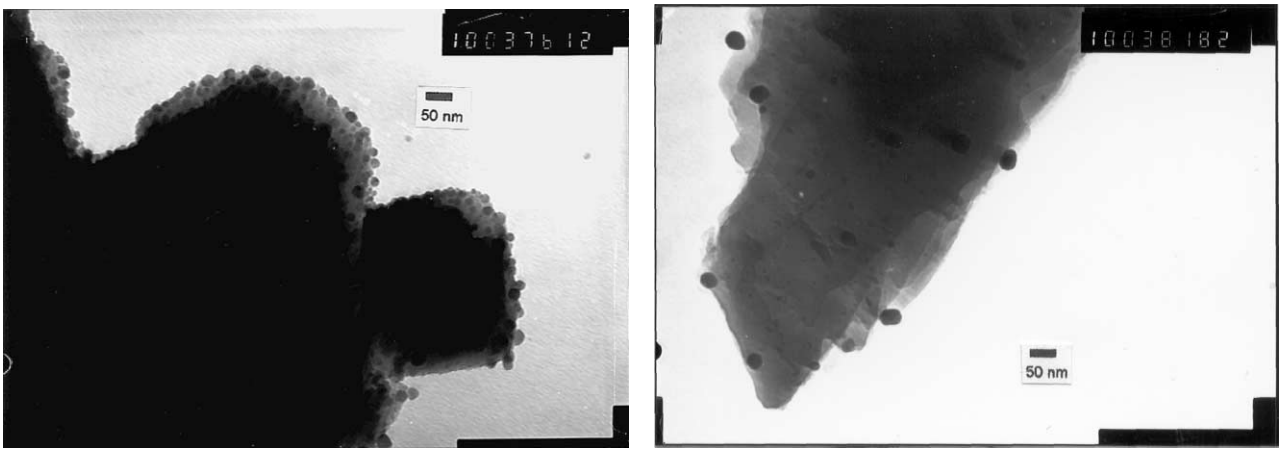

(a) (b)

Figure 2. TEM images of (a) HMCM-22 zeolite supported NiB amorphous alloy (10 wt% NiB/HMCM-22) and (b) Ni catalysts (10 wt% Ni/HMCM-22).

characterizations using TEM, XRD and XPS were carried out. TEM was employed to measure the metal particle size of the catalysts and XRD was used for crystalline phase identification. TEM measurements show that the metal particles are in range between 3 and 15 nm with most particles smaller than 10 nm for the supported amorphous NiB alloy catalysts. The Ni catalysts prepared by the standard incipient wetness impregnation method, offer relatively large metal particles with most particles larger than 15 nm. Figure 2 shows the TEM images of HMCM-22 supported NiB amorphous alloy and Ni catalysts. On the 10 wt% NiB/HMCM-22, the sizes of NiB amorphous alloy particles are found to range between 5 and 15 nm with most particles smaller than 10 nm. On the 10 wt% Ni/HMCM-22, the particle sizes are found in the range of 25–40 nm. Figure 3 shows the XRD patterns, which were obtained by subtracting the patterns of the corresponding supports from those of as-prepared catalysts. Only very weak broad peaks at 44.7° appear for the supported NiB catalysts, strongly indicating the typical amorphous structure of the metal particles. In contrast, sharp peaks at 44.6° are observed over the several supported nickel catalysts prepared by the standard incipient wetness impregnation method, suggesting the long-range order structure of the metal particles. XPS measurements show that the Ni 2p binding energy of 853.2 eV for the 10 wt% NiB/HMCM-22 catalyst is higher than those for pure metallic Ni (Ni 2p BE of 852.8 eV) and corresponding Ni catalyst (Ni 2p BE of 852.9 eV), suggesting that Ni for the NiB/HMCM-22 catalyst is electron-deficient. Such increase of nickel's binding energy had been observed by other research groups [9].

The above results suggest that the good catalytic behavior of the supported NiB amorphous alloy catalyst on the formation of a C–C bond between carbon species arising from decomposition of CH_4 can be contributed to its nanosize and amorphous structure as well as electron-deficient property.

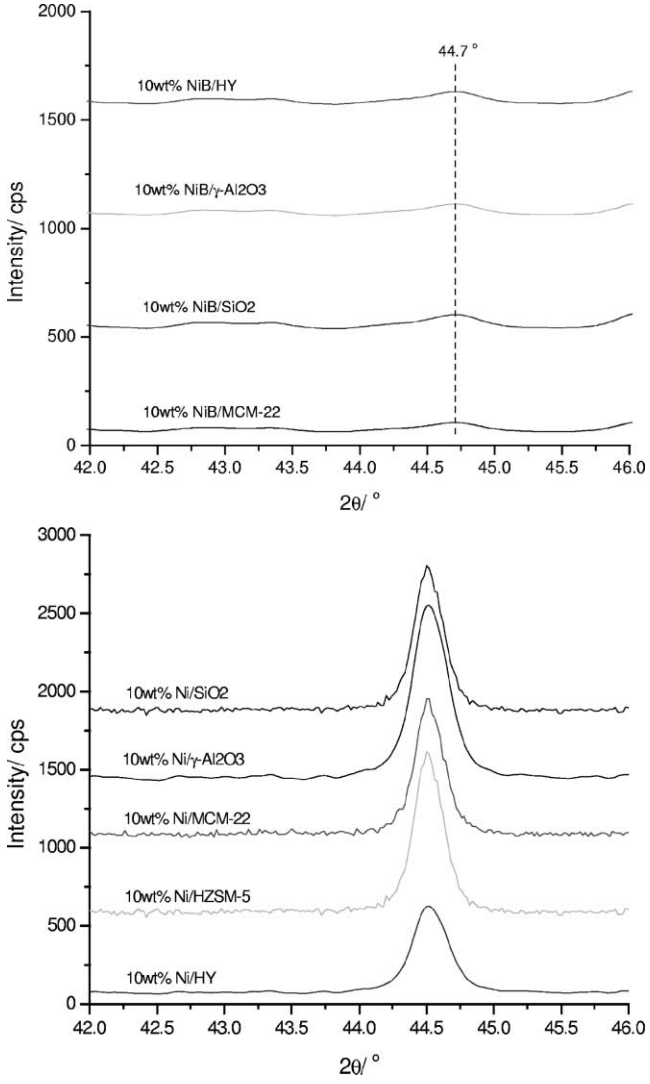

Figure 3. Subtracted XRD patterns of as-synthesized catalysts.

3.3. Correlation between the acidity of supports and catalytic performance

Figure 1 also shows that the yield of C_2 and C_3 hydrocarbons depends on the support and decreases in the following sequence: HMCM-22, HZSM-5 > HY > SiO_2, NaY > γ-Al_2O_3. The sequence of the specific surface area of such supports orders as follows: HY, NaY > SiO_2, HMCM-22, HZSM-5 > γ-Al_2O_3. Clearly, no definite correlation between the specific surface area and the reaction results can be obtained in this work.

However, the supports used in this work can be separated into three groups based on the acidity property of the support. The proton exchanged HMCM-22, HZSM-5, and HY have Brønsted acid sites. The γ-Al_2O_3 oxide shows Lewis acid sites. SiO_2 and NaY are non-acidic supports. Correlated with the results in figure 1, it can be found that zeolite-acidic supports give highest yields of C_2 and C_3 hydrocarbons during the hydrogenation in *step II*. Non-acidic supports give better C_2 and C_3 hydrocarbons yield than the Lewis acidic γ-Al_2O_3 support catalyst does. Moreover, it is well known that the acidic strength of the HMCM-22 (SiO_2/Al_2O_3 ratio 50), HZSM-5 (SiO_2/Al_2O_3 ratio 60) and HY supports orders in the following sequence: HMCM-22 $\approx$ HZSM-5 > HY, which correlates well with the sequence of the yield of C_2 and C_3 hydrocarbons. This may be ascribed to the enhancement of the acid catalyzed oligomerisation due to acidic strength high enough for HMCM-22 and HZSM-5 to activate the CH_4 molecule.

3.4. Hydrogen release in step I and hydrogenation rate of carbon in step II

Figure 4 shows the relationship between the H_2 yield and the conversion of CH_4 as well as the yield of carbon in *step I*. Clearly, the yield of H_2 is very close to that of carbon in

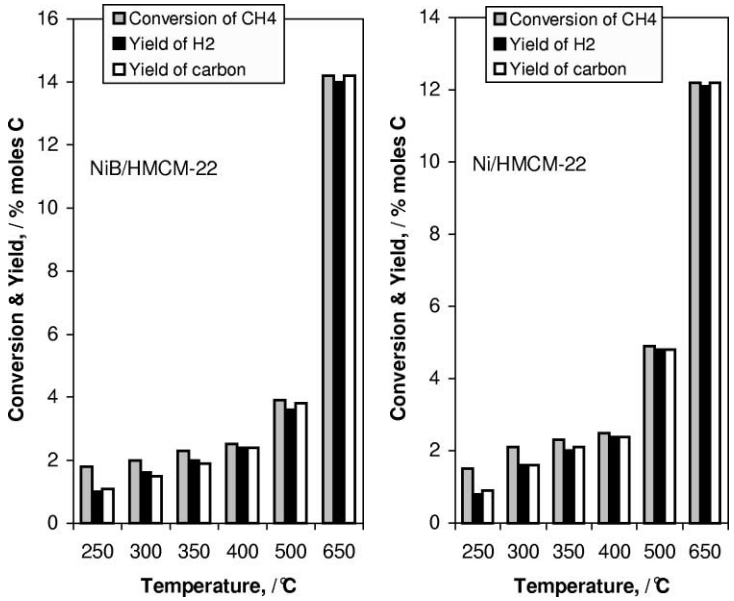

Figure 4. Relationship between the H_2 yield and the conversion of CH_4 as well as the yield of carbon in *step I*.

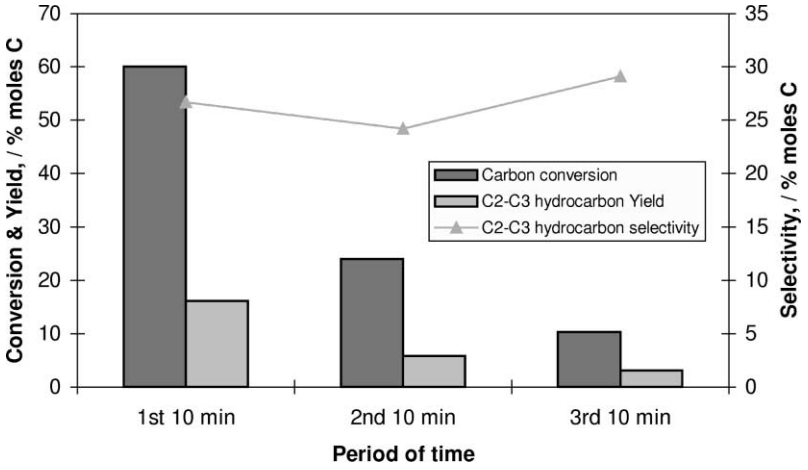

Figure 5. Yield and selectivity of C_2 and C_3 hydrocarbons, carbon hydrogenated at 300 °C during different hydrogenation periods for 10 wt% NiB/HMCM-22. Before hydrogenation, the catalyst was reacted with CH_4 at 300 °C for 10 min.

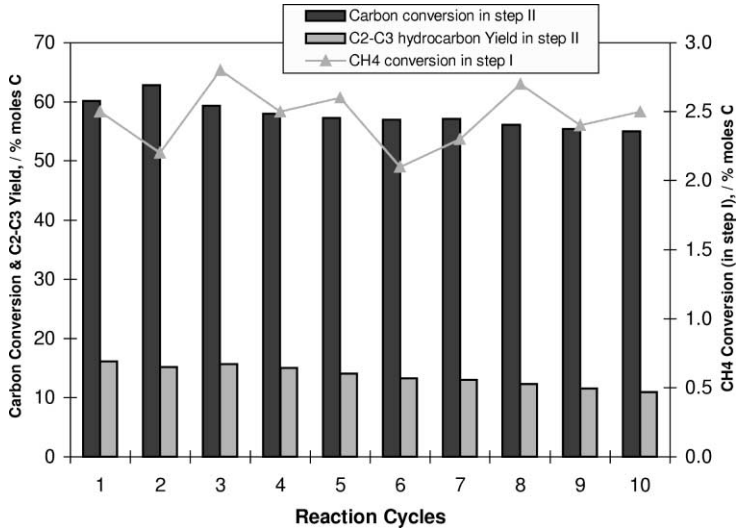

Figure 6. C_2 and C_3 hydrocarbons yield, methane conversion, and carbon hydrogenated as a function of reaction cycles for 10 wt% NiB/HMCM-22 catalyst at 300 °C. Data for C_2 and C_3 hydrocarbons yield and carbon hydrogenated were collected after a 10 min hydrogenation.

the decomposition of CH_4 (*step I*) in the whole temperature range. The results suggest that hydrogen formed from decomposition of CH_4 can easily escape from the catalyst surface. And, the carbon-containing species formed from decomposition of CH_4 is quite deficient in hydrogen, which is also supported by the fact that no signals of CH_x (x = 1–3) could be detected over the CH_4-reacted samples by FT-IR (Perkin–Elmer 2000 FT-IR) and Raman (RENISHAW 1000). This is in agreement with the results reported by Belgued *et al.* [2] over a standard Pt/SiO_2 catalyst. Actually, many contributions on single crystals showed that different forms of elemental carbon are favored at high temperature [11–14] and the stability of CH_x species is questioned beyond 127 °C [14,15].

Figure 5 shows the results of hydrogenation of carbon in different period of time. In the first 10 min, only 60.1% of the carbon formed from CH_4 decomposition is removed via hydrogenation with a yield of C_2 and C_3 hydrocarbons of 16.1%. In the second 10 min, another 24.3% of the total carbon is gasified with a yield of C_2 and C_3 hydrocarbons of 5.8%. After 30 min hydrogenation, 94.3% of total carbon formed in *step I* is gasified with a total yield of C_2 and C_3 hydrocarbons of 24.9%. The results indicate that the hydrogenation rate of carbon is not so fast as the decomposition rate of CH_4 (*step I*). In addition, the selectivity of C_2 and C_3 hydrocarbons maintains about 26% in the whole period of hydrogenation.

3.5. Multiple reaction cycles

Multiple-reaction-cycle tests were performed to examine the lifetime of the 10 wt% NiB/HMCM-22 catalyst. Each cycle of the reaction consists of two steps: 10 min methane decomposition, resulting in the production of H_2 and surface carbon species, and 10 min hydrogenation of such surface carbon. The yield of C_2 and C_3, methane conversion and carbon hydrogenated for MCM-22 zeolite supported NiB amorphous alloy catalyst of multiple reaction cycles is illustrated

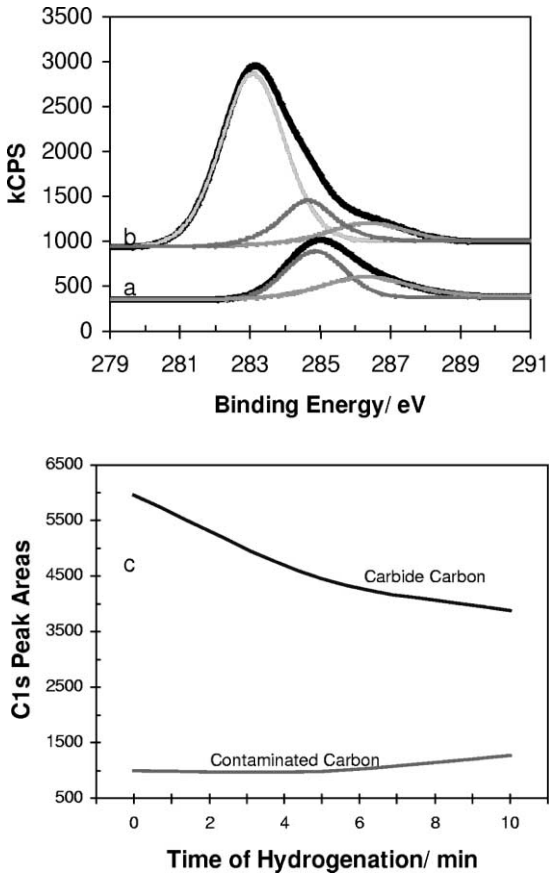

Figure 7. XPS spectra of 10 wt% NiB/HMCM-22 in the C 1s region for (a) fresh, (b) after 10 min exposure of CH_4 at 300 °C, and (c) C 1s peak areas of carbide carbon and contaminated carbon as a function of the time of hydrogenation.

in figure 6. The yield of C_2 and C_3 hydrocarbons decreases by about a third of the initial yield after ten reaction cycles. At the same time, methane conversion as well as the percentage of carbon hydrogenated decrease slightly. Koerts and van Santen [3,7] indicated that for C_{2+} formation it is important to have a high selectivity for C_α carbon formation and pointed out that it can be obtained at a low carbon surface coverage. In the present work, only ~60% of carbon can be gasified *via* hydrogenation in each cycle. Clearly, this means that the carbon surface coverage increases with the increase in the reaction cycles, so as to lower the selectivity for C_α surface carbon formation and in turn reduce the total yield of C_{2+} formation. In addition, Goodman and Koranne [4] suggested that the nature of intermediates may be affected by the presence of "inactive" carbon, which leads to decrease in C_2 and C_3 hydrocarbons selectivity.

3.6. XPS and TPSR studies

XPS spectra of the 10 wt% NiB/HMCM-22 catalyst in the C 1s region are displayed in figure 7. In comparison with the fresh HMCM-22 supported NiB catalyst, a strong C 1s peak at 283.4 eV which is assigned to nickel carbide carbon appears for the catalyst exposed to CH_4 for 10 min at 300 °C. Series of XPS measurements were carried out to study the hydrogenation of the carbide carbon. Upon the exposure of the surface carbide to hydrogen, the carbide carbon peak area decreases almost linearly with increasing the time of hydrogenation while the contaminated carbon remained almost constant (see figure 7(c)).

H_2-TPSR profiles for the 10 wt% NiB/HMCM-22 catalyst which was exposed to CH_4 for 10 min at 300 °C prior to the hydrogen treatment are illustrated in figure 8. As can be seen, the main product is CH_4, accompanied by a small

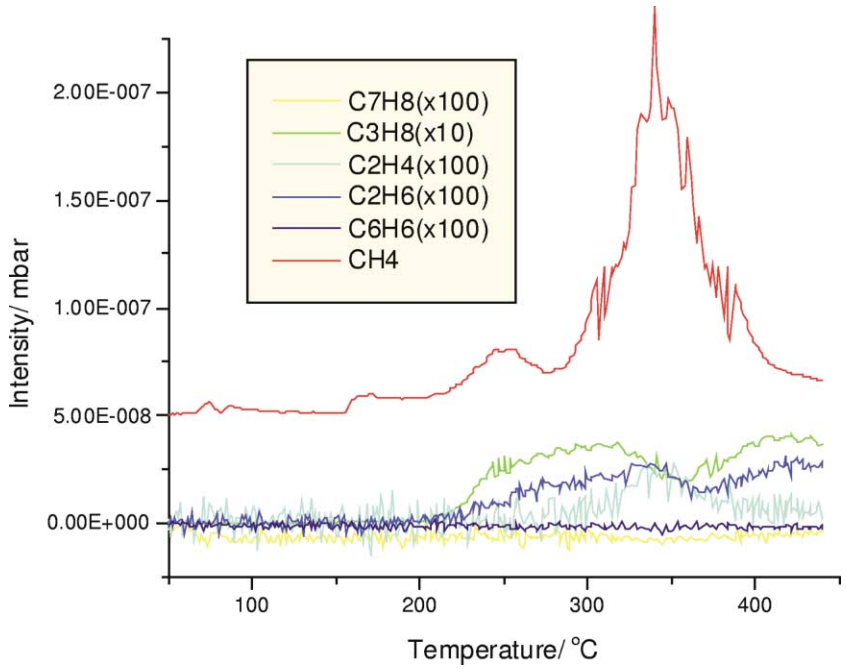

Figure 8. H_2-TPSR profiles following exposure of 10 wt% NiB/HMCM-22 catalyst to CH_4 at 300 °C for 10 min.

amount of propane and by traces of ethane and ethylene. The CH_4 profile consisted of a small peak at around 220 °C, and a large peak at around 300 °C. These two peaks are assigned to the carbide-like or carbide carbon as observed by the XPS. C–C bond formation to produce C_2 and C_3 hydrocarbons occurs at temperature higher than 200 °C with a maximum value at about 300 °C, which is consistent with the reaction data.

The above results indicate that carbide(-like) carbon is active and selective for hydrogenation resulting in the production of C_2 and C_3 hydrocarbons.

4. Conclusion

Methane conversion to hydrogen and higher hydrocarbons via a two-step, oxygen-free route was investigated for Ni–B amorphous alloy and Ni catalysts supported on HMCM-22, HZSM-5, HY, γ-Al_2O_3, and SiO_2. All catalysts give similar methane conversion and yields of hydrogen and H-deficient carbon-containing species in *step I* as well as similar carbon conversion in *step II*. The yields of C_2 and C_3 hydrocarbons depend greatly on the structure of the metal particles and support acidity. Supported NiB amorphous alloy catalysts offer higher yields of C_2 and C_3 hydrocarbons than the corresponding Ni catalysts do, which is due to nanoscale size, short-range disorder in structure, and electron-deficiency. Of the zeolite supported catalysts, the most strongly acidic HMCM-22 and HZSM-5 supported catalysts produce more C_2 and C_3 hydrocarbons than the zeolite HY supported catalyst. For the 10 wt% NiB/HMCM-22 catalyst, at 300 °C 60.1% of the carbon formed from CH_4 decomposition can be converted *via* hydrogenation with a 16.1% yield of C_2 and C_3 hydrocarbons during 10 min hydrogenation. Increasing hydrogenation time to 30 min, 94.3% of total carbon formed in *step I* is gasified with a total yield of C_2 and C_3 hydrocarbons of 24.9%. In addition, when tested for multiple reaction cycles, this catalyst shows a rather slow deactivation and further improvements in the catalyst lifetime are necessary in order for this process to be commercially attractive. High temperatures favor CH_4 decomposition and H_2 production in *step I*, but high temperatures make the subsequent hydrogenation of carbon formed from CH_4 decomposition difficult because of high carbon surface coverage and the presence of "inactive" carbon. XPS and H_2-TPSR measurements indicate that carbide(-like) carbon is active for hydrogenation, in which C–C bond formation to produce C_2 and C_3 hydrocarbons occurs at temperature higher than 200 ^{o}C with a maximum value at about 300 °C.

Acknowledgement

Financial support from ABB Lummus Global Inc. is gratefully acknowledged.

References

[1] M. Belgued, A. Amariglio, P. Pareja and H. Amariglio, J. Catal. 159 (1996) 441.
[2] M. Belgued, A. Amariglio, P. Pareja and H. Amariglio, Nature 352 (1991) 789.
[3] T. Koerts and R.A. van Santen, J. Chem. Soc. Chem. Commun. (1991) 1281.
[4] M.M. Koranne and D.W. Goodman, in: *Methane and Alkane Conversion Chemistry*, eds. M.M. Bhasin and D.W. Slocum (Plenum, New York, 1995) p. 49.
[5] M. Belgued, A. Amariglio, P. Pareja and H. Amariglio, J. Catal. 159 (1996) 449;
P. Pareja, S. Molina, A. Amariglio and H. Amariglio, Appl. Catal. A 168 (1998) 289;
M. Belgued, A. Amariglio, P. Pareja, H. Amariglio and J. Saint Just, Catal. Today 13 (1992) 437;
E. Mielczarski, S. Monteverdi, A. Amariglio and H. Amariglio, Appl. Catal. A 104 (1993) 215.
[6] M.M. Koranne and D.W. Goodman, Catal. Lett. 30 (1995) 219;
M.-C. Wu and D.W. Goodman, Catal. Lett. 24 (1994) 23;
M.-C. Wu, Q. Xu and D.W. Goodman, J. Phys. Chem. 98 (1994) 5104.
[7] T. Koerts and R.A. van Santen, J. Catal. 138 (1992) 101.
[8] F. Solymosi, A. Erdöhelyi and J. Cserényi, Catal. Lett. 16 (1992) 399;
A. Erdöhélyi, J. Cserényi and F. Solymosi, J. Catal. 141 (1993) 287.
[9] Y. Chen, Catal. Today 44 (1998) 3.
[10] Y. Lu, C. Yu, J. Xue, Y. Liu and S. Shen, Chem. Lett. (1997) 515.
[11] W. Hally, H.J. Bitter, K. Seshan, J.R.H. Ross and J.A. Lercher, Stud. Surf. Sci. Catal. 88 (1994) 167.
[12] T.P. Beebe Jr., D.W. Goodman, B.D. Kay and J.T. Yates Jr., J. Chem. Phys. 87 (1987) 2305.
[13] A.C. Luntz and D.S. Bethune, J. Chem. Phys. 90 (1989) 1274;
A.C. Luntz and J. Harris, J. Surf. Sci. 285 (1991) 397;
J. Harris, J. Simons, A.C. Luntz, C.B. Mullins and C.T. Rettner, Phys. Rev. Lett. 67 (1991) 652.
[14] I. Chorkendorff, I. Alstrup and S. Ullmann, Surf. Sci. 227 (1990) 291.
[15] Y.N. Wang, R.G. Herman and K. Klier, Surf. Sci. 279 (1992) 33.